

Translational Boundaries as Incipient Ferrielectric Domains in Antiferroelectric PbZrO₃

Ying Liu^{1,*}, Ranming Niu^{2,3}, Andrzej Majchrowski⁴, Krystian Roleder⁵, Kumara Cordero-Edwards¹,
Julie M. Cairney^{2,3}, Jordi Arbiol^{1,6}, and Gustau Catalan^{1,6,†}

¹*Catalan Institute of Nanoscience and Nanotechnology (ICN2), Campus Universitat Autònoma de Barcelona, Bellaterra 08193, Spain*

²*School of Aerospace, Mechanical and Mechatronic Engineering, The University of Sydney, Sydney, New South Wales 2006, Australia*

³*Australian Centre for Microscopy and Microanalysis, The University of Sydney, Sydney, New South Wales 2006, Australia*

⁴*Institute of Applied Physics, Military University of Technology, Ulica Kaliskiego 2, 00-908 Warsaw, Poland*

⁵*Institute of Physics, University of Silesia, Ulica 75 Pułku Piechoty 1, 41-500 Chorzów, Poland*

⁶*Institut Català de Recerca i Estudis Avançats (ICREA), Barcelona 08010, Catalunya, Spain*



(Received 11 October 2022; revised 26 February 2023; accepted 28 April 2023; published 25 May 2023)

In the archetypal antiferroelectric PbZrO₃, antiparallel electric dipoles cancel each other, resulting in zero spontaneous polarization at the macroscopic level. Yet in actual hysteresis loops, the cancellation is rarely perfect and some remnant polarization is often observed, suggesting the metastability of polar phases in this material. In this work, using aberration-corrected scanning transmission electron microscopy methods on a PbZrO₃ single crystal, we uncover the coexistence of the common antiferroelectric phase and a ferrielectric phase featuring an electric dipole pattern of $\downarrow\uparrow\downarrow$. This dipole arrangement, predicted by Aramberri *et al.* to be the ground state of PbZrO₃ at 0 K, appears at room temperature in the form of translational boundaries. The dual nature of the ferrielectric phase, both a distinct phase and a translational boundary structure, places important symmetry constraints on its growth. These are overcome by sideways motion of the boundaries, which aggregate to form arbitrarily wide stripe domains of the polar phase embedded within the antiferroelectric matrix.

DOI: [10.1103/PhysRevLett.130.216801](https://doi.org/10.1103/PhysRevLett.130.216801)

Antiferroelectrics are materials with an antiparallel but switchable alignment of electric dipoles of equal magnitude so that, in the absence of external voltage, the macroscopic net polarization is zero [1]. Historically, PbZrO₃ (PZO) was the first material proposed to be antiferroelectric [2,3], and is regarded as an archetype. Its electric dipoles arrange in a $\uparrow\uparrow\downarrow\downarrow$ fashion [Fig. 1(a)] [2]. For antiferroelectrics, applying a large enough electric field can rearrange the electric dipoles in the same direction, causing an antiferroelectric to ferroelectric transition identifiable by a characteristic double hysteresis loop in the polarization as a function of the electric field [3–5]. This antipolar-to-polar switching is accompanied by giant charge storage, volume expansion and temperature drop, and hence is promising in applications in high-density capacitors [6–8], high strain transducers [9,10], and electrocaloric cooling [11,12].

Closely related to antiferroelectrics, ferrielectric phases (characterized by possessing antiparallel but uncompensated electric dipoles) have also attracted attention [13–18]. They are reported to exist in different forms and under various conditions. For example, a $\uparrow\uparrow\downarrow\downarrow$ dipole pattern was observed in chemically doped PZO [15,19]; in pure PZO, antiparallel electric dipoles with imbalanced magnitude were theoretically predicted to exist under an electric field [13,14], and a more complex ferrielectric structure with a $\uparrow\uparrow\uparrow\uparrow\downarrow\uparrow\uparrow\downarrow$ dipolar configuration was also proposed based on a combination of *in situ* biasing x-ray

diffraction and simulation results [17]. Interestingly, even the ground state of PZO has been proposed to be ferrielectric instead of antiferroelectric, as *ab initio* calculations by Aramberri *et al.* [16] suggest that a $\downarrow\downarrow\uparrow\uparrow$ dipole pattern could be the lowest-energy state in PZO at 0 K and possibly up to room temperature where, being polar, it may contribute to the open double hysteresis loop in PZO [20,21]. Yet, this ferrielectric phase has not been experimentally observed.

In this Letter, we uncover the existence of domains of the $\downarrow\uparrow\downarrow$ ferrielectric phase in PZO single crystal at room temperature. The ferrielectric periodicity is one dipole smaller than the antiferroelectric one, and therefore intercalated ferrielectric layers fulfil the role of translational boundaries (TBs). TBs are discontinuities in the periodic modulation of the antiferroelectric lattice and are intrinsic topological defects in PZO [22–24]. A schematic explanation of such translational boundaries in antiferroelectrics is shown in Fig. 1(b). The concept can be understood by viewing the antipolar ordering as a square wave modulation of the polarization, with the period of the wave being equal to four perovskite unit cells (two dipoles in one direction and two in the opposite one). The translational boundaries [blue dotted lines in Fig. 1(b)] shift in the phase of this square wave by 1/4, 1/2, and 3/4 of the antiferroelectric (orthorhombic) unit cell, corresponding, respectively, to one, two, or three pseudocubic building blocks. Domains

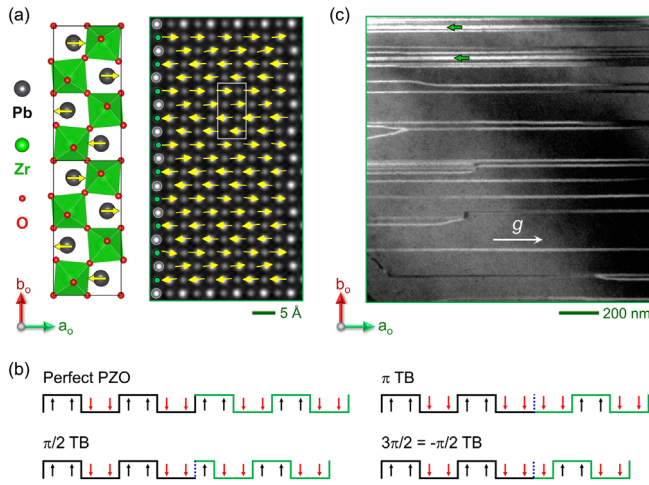


FIG. 1. (a) A structure model of PZO (two unit cells outlined by black rectangles) and a Pb displacement (Pb displacement with respect to their four nearest Zr, yellow arrows) map obtained from a STEM-HAADF image of the PZO single crystal visualized along the c_0 axis. (b) Schematics showing electric dipole arrangements and square waves representation of the perfect PZO, PZO with $\pi/2$, π , and $3\pi/2$ TBs. Blue dotted lines denote translational boundaries. (c) A transmission electron microscopy bright field image showing TBs observed in PZO single crystal. Green arrows indicate thicker TBs.

on either side of a translational boundary are thus related by phase shifts of $\pi/2$, π , and $3\pi/2$ [23,24]. The breaking of translational symmetry implies a local disruption of the perfect dipole cancellation, and antiphase boundaries in antiferroelectrics are expected to be polar [25]. Wei *et al.* proved the polar nature of antiphase boundaries (translational boundaries with a phase shift of π) in 2014, and highlighted their potential in information storage applications [22].

Ferrielectric phases and translational boundaries thus share commonalities. Both are closely related to, and can appear within, antiferroelectrics, while at the same time

being polar. In this Letter, we show that, in pure PZO, the ferrielectric Ima2 phase predicted to be the ground state of this material, exists at room temperature forming stripe domains that also act as translational boundaries of varying thickness and with phase shifts that are integer multiples of $\pi/2$.

A single crystal of PZO was used as the sample for this study. Details of the single crystal fabrication method are provided elsewhere [26]. Electron-transparent lamellae were cut from the crystal using focussed ion beam lithography. The lamellae were heated up to 250 °C and cooled down to favor the nucleation of different domains. Heated up to a lower temperature such as 150 or 200 °C can also cause the nucleation of new ferrielectric domains close to ferroelastic domain walls (Fig. S1 in the Supplemental Material [27]), suggesting that mechanical strain may lower the barrier for their formation, consistent with their extended presence in epitaxial thin films [28].

The samples show the expected antiferroelectric structure of PZO [Fig. 1(a)], but also extended planar structures [Fig. 1(c)]. These are similar to those observed by Wei *et al.* [22], who identified them as π translational boundaries, i.e., boundaries that change the phase of the dipole arrangement by a factor of π . We found, however, that the linear structures in the sample can have different thicknesses. Green arrows have been added in Fig. 1(c) to mark some thicker ones. Further atomic-scale investigations of these striplike features, displayed in Figs. 2–4, show that they are in fact ferrielectric domains that act de facto as translational boundaries with different phase angles multiple of $\pi/2$.

Figure 2(a) displays a scanning transmission electron microscopy high angle annular dark field (STEM-HAADF) image of the thinnest translational boundaries found in the PZO single crystal. Pb displacements (δ_{Pb}) with respect to their four nearest Zr were extracted using Python with the “Atomap” library [29]. The obtained δ_{Pb} map was superimposed on the corresponding STEM-HAADF image.

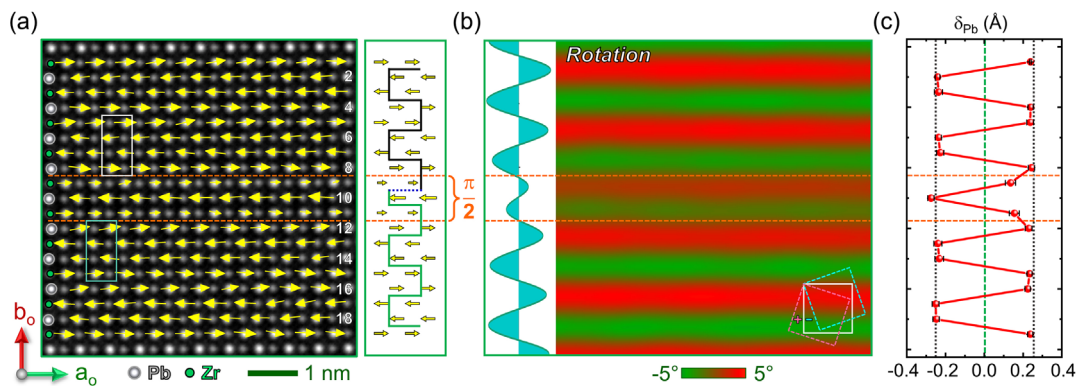


FIG. 2. (a) A Pb displacement map superimposed on the corresponding STEM-HAADF image showing a TB separating regions with $\pi/2$ difference in phase (along b_0 direction). (b) The GPA lattice rotation map of (a). The blue inset curve is an intensity profile of the lattice rotation map. (c) The Pb displacement curve by averaging rows from 1 to 19. Error bars, standard deviation. Black dotted lines, Pb displacement in ideal antiferroelectric PZO.

From the δ_{pb} map, a disturbance of antiferroelectric order can be observed. Electric dipoles arrange in the $\uparrow\uparrow\downarrow\downarrow\uparrow\uparrow$ manner, where an upward dipole is missed, and the single unpaired dipole is larger in magnitude. On both sides of this dipole, the antiferroelectric domains have a phase difference of $\pi/2$ and a relative shift of $1/4$ orthorhombic unit cells (i.e., one perovskite unit cell) along the orthorhombic **b** direction. We henceforth identify this ferrielectric structure as a $\pi/2$ TB.

We have also examined the lattice rotations by means of geometric phase analysis (GPA) [30,31] on the atomic resolution STEM-HAADF images. GPA is a method to determine lattice strain and rotation from high-resolution images [32,33]. A GPA lattice rotation map from Fig. 2(a) is shown in Fig. 2(b). The rotation angle at the TB region and its modulation period are smaller than in other upper and lower regions. The intensity profile indicates this trend. Based on this characteristic in GPA, it is possible to identify the TB even without a δ_{pb} map. It is also to be noted that GPA gives precise strain or lattice rotation values when analyzing long-range continuous strain. AFE PZO and TBs show short-range lattice modulations: the rotation angles change abruptly between neighboring lattices and the corresponding values are therefore discrete. When applying GPA to PZO, the resulting lattice rotation map is sinusoidal-like [Fig. 2(b)], because GPA defines lattice rotation at each pixel and its intrinsic averaging effect [34]. Even so, our results show the effectiveness of the GPA in determining the short-range modulation period and amplitude, and locating the TBs.

Quantitative analysis also shows that the magnitude of the middle unpaired electric dipole of the TB is bigger than the two satellite dipoles on either side, i.e., the dipolar structure is $\downarrow\uparrow\downarrow$. This means that, though the internal symmetry of the $\pi/2$ translational boundary is polar, its net polarization can be positive, negative, or zero depending on the relative difference between the central dipole and the sum of the two satellites. Moreover, we find that this relative ratio can change continuously within the same TB. For example, on the far left of the TB of Fig. 2(a), the middle δ_{pb} (0.25 Å) is smaller than the sum of the satellite dipoles (−0.17 and −0.21 Å, respectively), while on the far right of the TB, the middle dipole (δ_{pb} , 0.31 Å) is bigger than the sum of the two satellites (δ_{pb} , −0.07 and −0.15 Å, respectively).

In fact, despite the TB unit cell being polar, we find that the average polarization is close to zero. The averaged δ_{pb} plot as a function of the atomic rows is shown in Fig. 2(c). The middle δ_{pb} (0.275 Å) is a little bigger than that in the antiferroelectric region and in the ideal PZO model (black dotted lines), while the satellite δ_{pb} (average values of 0.135 and 0.155 Å) are much smaller than the middle δ_{pb} , but the sum of the two (0.135 + 0.155 = 0.290 Å) is almost equal the antiparallel displacement of the central dipole (0.275 Å). The conclusion from this analysis is that the

TB can change its internal polarization from positive to negative or even zero while still preserving the relative sign of the internal displacements, i.e., modulating only their relative magnitude. This is a qualitative difference with respect to ferroelectrics, for which inverting the sign of polarization requires inverting the sign of the atomic displacements within the unit cell. The ability to modulate the sign of the polarization without having to overcome a discrete energy barrier means that the internal polarization of the TBs can adapt to local variations in electric fields.

In addition to the $\pi/2$ TB, we have also observed TBs with two and three $\downarrow\uparrow\downarrow$ dipole units [Figs. 3(a) and 3(b)]. By extrapolating the antiferroelectric domains across these regions, we see that the square waves that represent the antipolar modulation on both sides of the TBs shift by a period difference of $1/2$ [Fig. 3(a)] and $3/4$ [Fig. 3(b)], respectively, so these are TBs with phase differences of π and $3\pi/2$. Translational boundaries with four or more $\downarrow\uparrow\downarrow$ dipole units have never been considered in previous research, yet they are also observed in our experiment. Figures 3(c)–3(e) show the superimposed STEM-HAADF micrographs + δ_{pb} maps and GPA lattice rotation maps for wider TBs. From these images, four [Fig. 3(c)], five [Fig. 3(d)], and seven [Fig. 3(e)] $\pi/2$ TB structural units can be determined.

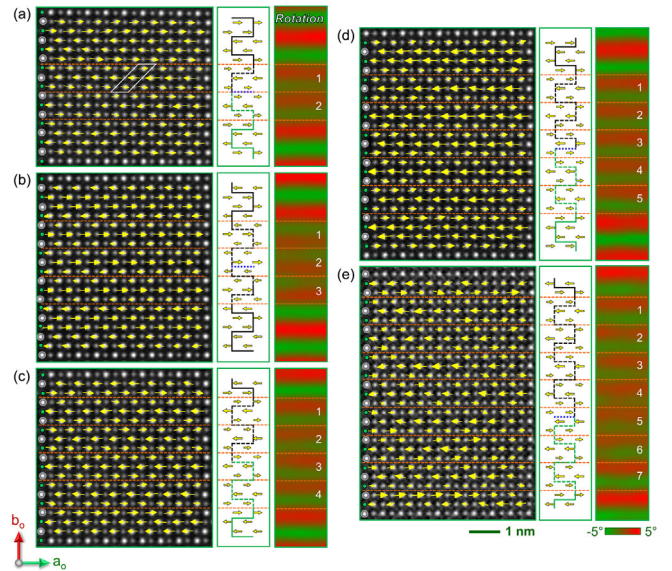


FIG. 3. TBs or ferrielectric phases observed in PbZrO_3 single crystal with (a) two, (b) three, (c) four, (d) five, and (e) seven $\downarrow\uparrow\downarrow$ structural units, corresponding to phase differences of π , $3\pi/2$, 0 , $\pi/2$ and $3\pi/2$, respectively. A ferrielectric structural unit is outlined by a white parallelogram in (a). A superimposed STEM-HAADF image + Pb map, a Pb displacement schematic and a GPA lattice rotation map are included in each panel. In Pb displacement schematics, the square waves are extended from outside (solid lines) to inside (dashed lines) of TBs until they meet, showing phase differences of π , $3\pi/2$, 0 , $\pi/2$, $3\pi/2$, respectively. TBs, blue dotted lines.

The formation of $\pi/2$, π , and $3\pi/2$ TBs is theoretically justified: they are topologically inevitable whenever adjacent antiferroelectric domains nucleate at atomic sites separated by a noninteger multiple of 4 perovskite unit cells along the polar-modulation direction. They are topologically protected because, to eliminate a TB, it is necessary to change the phase (and thus rearrange the dipoles) of at least one of the adjacent antiferroelectric domains. In contrast, TBs with a phase difference of 2π (equal to four $\pi/2$ TBs), such as in Fig. 3(c), do not enjoy such topological protection as there is no phase difference between the adjacent domains. Put another way: 4 $\downarrow\uparrow\downarrow$ dipole units can be replaced by 3 $\downarrow\uparrow\downarrow$ antiferroelectric dipole units without disturbing the translational symmetry of the adjacent domains. Likewise, five or seven $\pi/2$ TB can, in theory, be replaced by one antiferroelectric structural unit plus one or three $\pi/2$ TB structural units, which would in principle lower the crystal's energy if the antiferroelectric state was the ground state.

At this point, then, it becomes necessary to reexamine whether these structures should still be regarded as translational boundaries. They can also be viewed as domains of a ferrielectric phase ($\downarrow\uparrow\downarrow$) embedded within the antiferroelectric matrix ($\downarrow\uparrow\downarrow\downarrow$). Since the thicker stripes are not a topological necessity, their existence suggests that the free energy of the ferrielectric phase must be sufficiently low to be at least locally stable at room temperature. Indeed, the three-dipole arrangement of the TBs is the same unit cell proposed by Aramberri *et al.* [16] as the theoretical ground state of PZO.

The dual nature of the FiE phase (both a separate phase and a translational boundary structure) also means that its growth is topologically hindered by the translational symmetry of AFE matrix. Nucleating new FiE domains at room temperature is nevertheless possible: we have observed it to happen as boundaries around small needle-like antiferroelectric domains (yellow arrow in Fig. 4), typically nucleating near lattice discontinuities such as

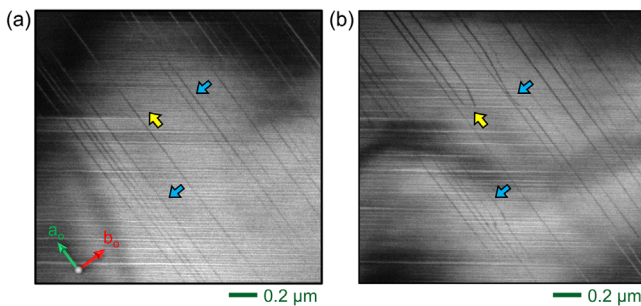


FIG. 4. Nucleation and movement of FiE regions at room temperature, induced by sustained electron irradiation inside the TEM. (a) As prepared TEM sample. (b) after intense electron beam irradiation. The yellow arrow shows a new FiE stripe as the TB around a needlelike AFE domain. The upper blue arrows show the FiE stripe movements.

interfaces or twin walls (Supplemental Material [27], Fig. S1). Note that the continuity of the AFE matrix dictates that the two TBs that bound such needles must have a combined phase difference that is an integer multiple of 2π . The electron-beam-induced motion of the FiE domains was also observed (blue arrows in Fig. 4), showing that the ferrielectric phase is sensitive to electric fields [28].

In order to fully characterize the ferrielectric unit cell, it is necessary to determine its oxygen positions. In STEM-HAADF images, only Pb and Zr can be observed. Instead, we turn to STEM integrated differential phase contrast (IDPC) imaging, which is sensitive to light elements [35] and can image oxygen in perovskite oxides [36]. The results for a $\pi/2$ and π TB are shown in Figs. 5(a) and 5(b), respectively. A primitive cell is outlined using a white parallelogram in Fig. 5(a). Along the \mathbf{a}_0 direction, all horizontal oxygen chains are slightly rippled, and tilt in opposite directions on both sides of the biggest Pb displacements (central dipole in the TB structural units). Along the \mathbf{b}_0 direction, the tilting pattern is $/ - | - \backslash$, that is, clockwise, straight, anticlockwise, with the central (bigger) dipole coinciding with the untilted oxygen chain and showing the characteristic anticorrelation between tilts and polarizations in perovskites. A unit cell was outlined by a white rectangle in Fig. 5(b). The structural model built according to experimental results and optimized using density functional theory is shown in Fig. 5(c) (more

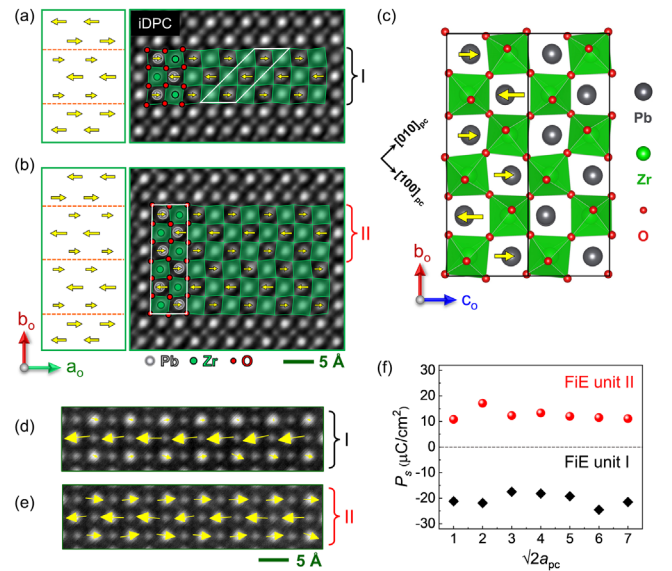


FIG. 5. (a),(b) STEM-IDPC images showing Pb, Zr, and O distribution at $\pi/2$ and π TBs, respectively. (c) The ferrielectric PZO model. Two unit cells are outlined using black rectangles. (d) The STEM-HAADF image of the same FiE unit as that labeled “I” in (a). (e) The STEM-HAADF image of the same FiE unit as that labeled “II” in (b). (f) Unit cell scale spontaneous polarization that was calculated based on the Pb, Zr, and O positions in the corresponding IDPC images.

details in Supplemental Material [27], Fig. S2). The space group of the optimized structure is also $Ima2$, the same as that reported in Ref. [16].

The HAADF images and superimposed δ_{Pb} map corresponding to the FiE unit I and II labeled in Figs. 5(a) and 5(b) are shown in Figs. 5(d) and 5(e), respectively. By extracting Pb, Zr, and O positions from iDPC images in Figs. 5(a) and 5(b), the polarization was quantitatively calculated using the Born effect charge method where $P_s = V^{-1} \sum_i \delta_i Z_i$ and shown in Fig. 5(f). The FiE unit I shows positive and the FiE unit II shows negative polarizations, despite both having the same orientation of the central dipoles [see Figs. 5(d) and 5(e)]. This result provides further evidence that the sign of polarization can change without switching the sign of Pb displacements. The Born effect charge used in the P_s calculation is from Ref. [22].

In terms of functionalities, since the FiE domains (TBs) are polar, and therefore piezoelectric and capable of optical second harmonic generation. They also may contribute to the small remnant polarization at 0 V often reported in the double hysteresis loops of PZO [20,21,37,38] but, given the uncertainty about the magnitude of their polarization, it is hard to quantify their contribution. The observation that polarization can easily vary in magnitude and sign within ferrielectric domains also suggests that these structures have high dielectric susceptibility and increasing their concentration may therefore be beneficial for capacitor applications. Since the FiE phase can be generated anytime the AFE phase is freshly nucleated, repeated field-induced switching of the antiferroelectric may result in a progressive accumulation of polar domains. This would manifest as an “antifatigue,” whereby the remnant polarization increases with the number of switching cycles; this is the opposite of ferroelectric fatigue, whereby polarization decreases with repeated switching. This “reverse fatigue” phenomenon of antiferroelectrics has been observed [39].

Ferrielectrics share some of the properties of antiferroelectrics (they are antipolar lattices that can be switched into a homogeneous polar state by application of an external voltage) and some of those of ferroelectrics (remnant polarization, piezoelectricity and so forth). As such, they are an exciting prospect for new concepts in multifunctional devices combining both functionalities, e.g., energy storage (antiferroelectric) and data storage (ferroelectric). Our work on single crystals suggests that PbZrO_3 is energetically close to being ferrielectric, with the FiE phase showing up as translational boundaries that aggregate to form wider stripe domains where the phase difference is larger than $3\pi/2$, the maximum topological value [22]. Here, topological protection acts as a double-edged sword: it guarantees the existence of FiE domains in the form of translational boundaries, but it complicates their growth precisely because of its impact on the translational symmetry of the AFE matrix. Overcoming this obstacle will require either finding a composition or strain state

where the FiE phase nucleates at a higher temperature than the AFE one, or else repeated switching in the hope that the progressive accumulation of TBs tilts the energy balance in favor of a homogeneous ferrielectric phase.

This project has received funding from the European Union’s Horizon 2020 research and innovation program under Grant Agreement No. 766726 (TSAR), in addition to Grant PID2019–108573 GB-C21 funded by MCIN/AEI/10.13039/501100011033. ICN2 acknowledges funding from Generalitat de Catalunya 2017 SGR 327. ICN2 is supported by the Severo Ochoa program from Spanish MINECO (Grant No. SEV-2017-0706) and is funded by the CERCA Programme / Generalitat de Catalunya. Y.L. acknowledges the BIST Postdoctoral Fellowship Programme (PROBIST) funded by the European Union’s Horizon 2020 research and innovation programme under the Marie Skłodowska-Curie Grant Agreement No. 754510. K.C. and A.M. acknowledge funding by the National Science Centre, Poland, Grant No. 2020/37/B/ST3/02015. The authors are grateful for the scientific and technical support from the Australian Centre for Microscopy and Microanalysis (ACMM) as well as the Microscopy Australia Node at the University of Sydney. Thanks Prof. Jorge Íñiguez and Dr. Hugo Aramberri from the Luxembourg Institute of Science and Technology (LIST) for the discussion of the space group and Glazer notation of the ferrielectric phase. Thanks to Ran Xu, from University Paris-Saclay, CentraleSupélec, CNRS, Laboratoire SOMS, for assistance in the geometric optimization of FiE PZO unit cell using density functional theory.

*ying.liu@icn2.cat

†gustau.catalan@icn2.cat

- [1] C. Kittel, *Phys. Rev.* **82**, 729 (1951).
- [2] E. Sawaguchi, H. Maniwa, and S. Hoshino, *Phys. Rev.* **83**, 1078 (1951).
- [3] G. Shirane, E. Sawaguchi, and Y. Takagi, *Phys. Rev.* **84**, 476 (1951).
- [4] X. Tan, C. Ma, J. Frederick, S. Beckman, and K. G. Webber, *J. Am. Ceram. Soc.* **94**, 4091 (2011).
- [5] P. Vales-Castro, M. Vellvehi, X. Perpiñà, J. M. Caicedo, X. Jordà, R. Faye, K. Roleder, D. Kajewski, A. Perez-Tomas, E. Defay, and G. Catalan, *Adv. Electron. Mater.* **7**, 2100380 (2021).
- [6] A. Chauhan, S. Patel, R. Vaish, and C. R. Bowen, *Materials* **8**, 8009 (2015).
- [7] Z. Liu, T. Lu, J. Ye, G. Wang, X. Dong, R. Withers, and Y. Liu, *Adv. Mater. Technol.* **3**, 1800111 (2018).
- [8] C. A. Randall, Z. Fan, I. Reaney, L.-Q. Chen, and S. Trolier-McKinstry, *J. Am. Ceram. Soc.* **104**, 3775 (2021).
- [9] W. Y. Pan, C. Q. Dam, Q. M. Zhang, and L. E. Cross, *J. Appl. Phys.* **66**, 6014 (1989).

- [10] S.-E. Park, M.-J. Pan, K. Markowski, S. Yoshikawa, and L. E. Cross, *J. Appl. Phys.* **82**, 1798 (1997).
- [11] R. Pirc, B. Rožič, J. Koruza, B. Malič, and Z. Kutnjak, *Europhys. Lett.* **107**, 17002 (2014).
- [12] P. Vales-Castro, R. Faye, M. Vellvehi, Y. Nouchokgwe, X. Perpiñà, J. M. Caicedo, X. Jordà, K. Roleder, D. Kajewski, A. Perez-Tomas, E. Defay, and G. Catalan, *Phys. Rev. B* **103**, 054112 (2021).
- [13] P. Tolédano and M. Guennou, *Phys. Rev. B* **94**, 014107 (2016).
- [14] P. Tolédano and D. D. Khalyavin, *Phys. Rev. B* **99**, 024105 (2019).
- [15] Z. Fu, X. Chen, Z. Li, T. Hu, L. Zhang, P. Lu, S. Zhang, G. Wang, X. Dong, and F. Xu, *Nat. Commun.* **11**, 3809 (2020).
- [16] H. Aramberri, C. Cazorla, M. Stengel, and J. Íñiguez, *npj Comput. Mater.* **7**, 196 (2021).
- [17] R. G. Burkovsky, G. A. Lityagin, A. E. Ganzha, A. F. Vakulenko, R. Gao, A. Dasgupta, B. Xu, A. V. Filimonov, and L. W. Martin, *Phys. Rev. B* **105**, 125409 (2022).
- [18] L. Qiao, C. Song, Q. Wang, Y. Zhou, and F. Pan, *ACS Appl. Nano Mater.* **5**, 6083 (2022).
- [19] T. Ma, Z. Fan, B. Xu, T. H. Kim, P. Lu, L. Bellaiche, M. J. Kramer, X. Tan, and L. Zhou, *Phys. Rev. Lett.* **123**, 217602 (2019).
- [20] L. Pintilie, K. Boldyreva, M. Alexe, and D. Hesse, *J. Appl. Phys.* **103**, 024101 (2008).
- [21] M. Guo, M. Wu, W. Gao, B. Suna, and X. Lou, *J. Mater. Chem. C* **7**, 617 (2019).
- [22] X. K. Wei, A. K. Tagantsev, A. Kvasov, K. Roleder, C. L. Jia, and N. Setter, *Nat. Commun.* **5**, 3031 (2014).
- [23] I. Rychetsky, W. Schranz, and A. Troster, *Phys. Rev. B* **104**, 224107 (2021).
- [24] X. K. Wei, C. L. Jia, K. Roleder, and N. Setter, *Mater. Res. Bull.* **62**, 101 (2015).
- [25] G. Catalan, J. Seidel, R. Ramesh, and J. F. Scott, *Rev. Mod. Phys.* **84**, 119 (2012).
- [26] J.-H. Ko, M. Górný, A. Majchrowski, K. Roleder, and A. Bussmann-Holder, *Phys. Rev. B* **87**, 184110 (2013).
- [27] See Supplemental Material at <http://link.aps.org/supplemental/10.1103/PhysRevLett.130.216801> for annealing induced new FiE phase nucleation and structure optimization details of the FiE phase.
- [28] R.-J. Jiang, Y. Cao, W.-R. Geng, M.-X. Zhu, Y.-L. Tang, Y.-L. Zhu, Y. Wang, F. Gong, S.-Z. Liu, Y.-T. Chen, J. Liu, N. Liu, J.-H. Wang, X.-D. Lv, S.-J. Chen, and X.-L. Ma, *Nano Lett.* **23**, 1522 (2023).
- [29] M. Nord, P. E. Vullum, I. MacLaren, T. Tybell, and R. Holmestad, *Adv. Struct. Chem. Imaging* **3**, 9 (2017).
- [30] M. J. Hytch, E. Snoeck, and R. Kilaas, *Ultramicroscopy* **74**, 131 (1998).
- [31] Y. Liu, Y. J. Wang, Y. L. Zhu, C. H. Lei, Y. L. Tang, S. Li, S. R. Zhang, J. Li, and X. L. Ma, *Nano Lett.* **17**, 7258 (2017).
- [32] Y. L. Tang, Y. L. Zhu, X. L. Ma, A. Y. Borisevich, A. N. Morozovska, E. A. Eliseev, W. Y. Wang, Y. J. Wang, Y. B. Xu, Z. Zhang, and S. J. Pennycook, *Science* **348**, 547 (2015).
- [33] Y. L. Tang, Y. L. Zhu, Y. Liu, Y. J. Wang, and X. L. Ma, *Nat. Commun.* **8**, 15994 (2017).
- [34] J. L. Rouvière and E. Sarigiannidou, *Ultramicroscopy* **106**, 1 (2005).
- [35] I. Lazić, E. G. T. Bosch, and S. Lazar, *Ultramicroscopy* **160**, 265 (2016).
- [36] Y. Liu, R.-M. Niu, S. D. Moss, P. Finkel, X. Z. Liao, and J. M. Cairney, *J. Appl. Phys.* **129**, 234101 (2021).
- [37] J. Ge, D. Remiens, X. Dong, Y. Chen, J. Costecalde, F. Gao, F. Cao, and G. Wang, *Appl. Phys. Lett.* **105**, 112908 (2014).
- [38] K. Boldyreva, D. Bao, G. L. Rhun, L. Pintilie, M. Alexe, and D. Hesse, *J. Appl. Phys.* **102**, 044111 (2007).
- [39] P. Mohapatra, D. D. Johnson, J. Cui, and X. Tan, *J. Mater. Chem. C* **9**, 15542 (2021).